IEEE Access
Multidisciplinary ⋮ Rapid Review ⋮ Open Access Journal

Received September 3, 2021, accepted October 17, 2021, date of publication October 22, 2021, date of current version October 28, 2021.

Digital Object Identifier 10.1109/ACCESS.2021.3122122

Performance Enhancement of an MTL Coil Loaded With High-Permittivity Dielectric Liner for 7 T Brain MRI

SANA ULLAH AND HYOUNGSUK YOO, (Senior Member, IEEE)
Department of Electronics Engineering, Hanyang University, Seoul 04763, Republic of Korea

Corresponding author: Hyoungsuk Yoo (hsyoo@hanyang.ac.kr)

This work was supported in part by the Institute for Information & Communications Technology Promotion (IITP) Grant funded by the Korean Government [Ministry of Science, ICT and Future Planning (MSIP)] (No. 2021-0-00490), and in part by the Development of Precision Analysis and Imaging Technology for Biological Radio Waves.

ABSTRACT In a multi-element microstrip transmission line (MTL) transmit array coil, the transmit field (B_1^+) distribution is inhomogeneous due to its standing-wave nature, and the interference effects can severely degrade the B_1^+ and imaging. Therefore, to improve the homogeneity and strength of B_1^+, this study focuses on the development of a multi-element MTL transmit array coil integrated with a dielectric liner (DL) material. Furthermore, the transmission efficiency ($T_{x,eff}$) is improved in the head region. An eight-element MTL transmits array head coil is investigated using thinner DLs, and the optimized dimensions of the DL are found from its resonant mode at 7 Tesla (T). Simulations and measurements are performed with an MTL transmit array coil at 7 T, and the performance is analyzed for the DL positions and dimensions. Remarkably, the proposed DLs-integrated transmit array coil system offered significant improvements in the $T_{x,eff}$ at different DLs positions. Compared to the case without the DL, the $T_{x,eff}$ is improved by 9% (DL close to the head model), 15% (DL at center), and 39% (DL close to the RF coil). Interestingly, the DL acts as an efficiency tuner element exhibiting a 9% to 39% $T_{x,eff}$ tuning range of improvement. In addition, the RF-shimming technique improves the B_1^+ homogeneity and $T_{x,eff}$ of the coil with DLs by 21% and 42%, respectively, compared to the case without the DL. Moreover, the specific absorption rate (SAR) analysis of the MTL transmit array coil with the DLs is performed. The peak 10g-averaged SAR is reduced from 3.1 W/kg to 2.13 W/kg in the head using DLs and RF-shimming technique. Finally, we used the bench measurement setup to obtain the measured magnetic field. The proposed work exhibits salient features with a smaller DL size and multi-element MTL transmit array coil than other proposed works.

INDEX TERMS 7 T, dielectric pad, eight-element, MTL transmit array, radio frequency (RF) coil, RF shimming, region of interest.

I. INTRODUCTION

Due to advancements in the magnetic resonance imaging (MRI) modalities, 7 Tesla (T) magnets are used to obtain high signal-to-noise ratio (SNR) and spatial resolution as compared to the 1.5 T and 3 T systems. However, at ultra-high-field (UHF) MRI, the wavelength becomes smaller than the human head and causes significant interference effects in the B_1^+, which can severely degrade the image quality [1], [2]. The interaction between the RF field and the human body can impose additional challenges such as the higher RF transmitter power and the RF power deposition or specific absorption rate (SAR) [3], [4]. Various types of coils such as birdcage (BC), microstrip transmission line (MTL), and surface coil are used in the UHF MRI. Among them, the MTL transmit array coils hold the potential to provide improved homogeneity and SNR [3]. An MTL transmits array coil contains MTL resonators, which are mutually decoupled and operated as independent transmit coils [3], [5]. The amplitude and phase of each resonator can be varied (B_1 shimming) to approach the desired transmit field (B_1^+) distributions [6], [7].

Previously, a different number of resonators have been used in MTL transmit array coil to improve the RF efficiency and B_1 shimming at UHF MRI in [8]–[10]. Moreover, other

The associate editor coordinating the review of this manuscript and approving it for publication was Tutku Karacolak.

techniques such as modifying the shape and geometry of the resonator [1], [11], the use of adjustable coils [12], and dielectric pads or dielectric liners (DL) were introduced. By modifying the shape of the resonators [1], [11] the overall field distribution was enhanced up to certain limits; however, the field intensity drastically decreased in the near field region due to the large distance between the coil and the human head. Thus, adjustable coils were used in [12]; nevertheless, the coil adjustment was manually controlled, which makes it time-consuming and impractical. On the other hand, the dielectric liner (DL) materials have been used as a convenient and feasible solution in many applications to improve the local sensitivity and/or homogeneity of the RF B_1^+ in human MRI systems [13]–[26]. Gel-based pads [13], aqueous [14], and simple dielectric materials [15], [16] were used to improve the field distribution in head imaging at 3 and 7 T. It is worth mentioning here that the BC coils were used in combination with these dielectric materials; however, in modern multichannel UHF MRI systems, the BC coil may be impractical for some applications requiring high B_1^+ homogeneity over the brain. Modern UHF MRI systems require multichannel coils in combination with the independent control of the phases and amplitudes of each channel independently to achieve a homogeneous magnetic field and high SNR, which is impossible in BC coils MRI due to its 2-channel configuration and fixed phase. Furthermore, the much thicker gels or aqueous water pads were placed inside the plastic bags, and their properties could change during an MRI scan [18]. A new deformable pad made of Calcium Titanate ($CaTiO_3$) powder mixed with water has shown good improvements in the area of the temporal lobe for brain imaging [23], but the pad had immense linear dimensions of 100 mm $\times$ 140 mm placed alongside the head. In [24], the dielectric materials have been used in combination with BC coil to resolve a signal drop-off issue in the right hemisphere of the brain. However, only a single large pad is placed at the right-hand side of the human head, which can only be used for specific head area imaging. A transceiver array coil was used with DL to increase the signal locally [25]; however, the investigated large cylindrical DL placed around the cylindrical phantom which can be useful for homogenous phantoms. The thick cylindrical shape of the DL makes it complicated for the heterogeneous human study. Recently, a dipole coil configuration was studied using the dielectric pad to improve the magnitude B_1 in [26]. Although the pad improved the B_1 homogeneity and magnitude, only a single dipole coil with a large size dielectric pad was used. Recently, in [27]–[30], DL and pads were investigated either for the reduction of mutual coupling between the channels or for the field improvement; however, the major drawbacks are that the RF coil is BC and the DL size is much larger.

Most of the above studies used larger pad sizes and different numbers of the pads near the target phantoms. Moreover, most of the dielectric pads used in the above studies are hard to maintain the specific dimensions and shapes; however, the radio frequency response and its fields are dependent on the shape and especially on the dimensions of the pads, which has been not studied yet. Similarly, several studies have focused on the effects of pads with the BC coil; yet, the pad effects with MTL transmit array coils had never been discussed in earlier literature. Furthermore, the pads used previously had large thickness, which limits the head-MRI bore area and sometimes hard to fit for big heads. Therefore, the thinner and compact DL with stable dielectric properties can be advantageous in multi-channel head-MRI systems.

This paper introduces solid ceramic-based thin DLs in combination with an eight-element MTL transmit array RF coil for the enhancement of transmission efficiency ($T_{x,eff}$) and field improvement. Moreover, in contrast with previous literature, the effect of DL size based on the operating frequency has been discussed. The DL size and position are the critical factors for the B_1^+ field enhancement. Further, the DL size should be optimized relative to the MTL coil size and operating frequency. The DLs with a small thickness of 0.5 cm, relative permittivity (ε_r) of 78, and conductivity (σ) of 0.0001 S/m were placed near the RF transmit coil. The $T_{x,eff}$ and the relative B_1^+ inhomogeneity of the coil without and with DL were calculated through the mean of the B_1^+ and coefficient of variation (CV), respectively. Additionally, the numerically generated MRI images were compared without and with the DLs for the SNR improvement. Finally, the proposed work was compared with previously related published papers of DLs in Table 1. The proposed DLs improved the field homogeneity and $T_{x,eff}$ by 21% and 39%, respectively, with a compact size and ultra-stable dielectric properties, which is suitable to use with MTL head coils.

II. MATERIALS AND METHODS

A. FULL-WAVE EM SIMULATIONS

Full-wave electromagnetic simulations were performed using a finite difference time domain (FDTD) simulator Sim4Life (v. 3.0.1.1201). The MRI RF coil configuration of interest is illustrated in Fig. 1(b) and consists of an eight-element head MTL transmit array coil array and a Duke body model. The Duke model consists of all the various tissues of the male body obtained from the virtual family dataset [31]. The RF transmit coil consists of the finite ground plane, a dielectric substrate, and MTL to transmit the RF field in the head model. Each element of the MTL transmit array coil was modeled by an MTL element on a low loss Teflon (PTFE) bar with $\varepsilon_r = 2.1$ and $\delta = 0.004$, height, width, and length of 1.8, 5, and 15 cm, respectively, as shown in Fig. 1(a). The resonant length of the microstrip element is foreshortened from $\lambda/2$ using capacitors ($C_p = 8.2$ pF and $C_t = 2.73$ pF) at the ends, and a matching capacitor ($C_m = 3.4$ pF) in series with the load. We used different values for the port and terminal capacitors to match the MTL array coil with the head, and after loading the Duke model, the C_t/C_m has been re-adjusted to achieve 50-ohm impedance matching.

Thereafter, a DL made of Barium samarium titanate (BaSmTi) oxide composition was designed for $T_{x,eff}$

TABLE 1. Comparison of the proposed high dielectric liner (DL) with prior work.

Ref.	Pad or DL	DL thickness (cm)	Permittivity value	RF Coil Type	MRI Tesla	Purpose of study
[13]	Gel pad	2	Skin (65)	Head birdcage	3T	Reduction of dielectric artifact
[14]	Water pad	4	78	Head TEM	7T	Manipulation of image intensity
[16]	Ultrasound gel or water	------	78	Body-array	3T	Improvements in image homogeneity
[17]	BaTiO3 in deuterated water	1	286	High-pass birdcage	7T	Improving spatial resolution of ear.
[21]	CaTiO3 with water	2	156	Head birdcage	7T	Tailoring the B1+
[23]	polyvinylchloride (PVC) with CaTiO3	1	110	Quadrature birdcage	7T	Medial lobe MRS improvements
[25]	BaTiO3 powder suspension	2	78, 150	Transceiver Array	4.7T	Increase the signal and homogeneity
[26]	CaTiO3 and D_2O oxide	1	110	Dipole coil	7T	Improve the $B1$ homogeneity
[27]	BaTiO3 powder suspension	------	150	Transceiver Array	4.7T	Maximize the homogeneity
[28]	MTM liner	1	-----	Birdcage coil	4.7T	SAR prevention
[29]	BaTiO3 and CaTiO3 powder with water	2	298, 110	Head birdcage	7T	Improving SNR and Transmission efficiency
[30]	BaTiO3 suspension	1.5	300	Birdcage coil	3T	Improving Homogeneity
This work	Barium samarium titanate (BaSmTi) oxide	0.5	78	MTL transmit array	7T	Improving Transmission Efficiency (39%)

improvement, as shown in Fig. 1(a). In the simulations, we used a dielectric liner having ε_r of 78 and conductivity (σ) 0.0001 S/m, while for the fabrication, we used the solid ceramic block made of BaSmTi to get our desired dielectric constant value in the lossless condition. The material is unique to MRI research and is highly soluble, which allows it to be modified in different ways. Two distinct DL sizes of 5 cm × 15 cm × 1 cm and 5 cm × 15 cm × 0.5 cm were evaluated to find the optimum size for the $T_{x,eff}$ improvement. It was found from the analysis of the resonant mode of the DL that the 0.5 cm provided one of the resonant modes at 298 MHz (7 T). Therefore, the thickness of the DL was set to 0.5 cm. Finally, the DLs were placed at three different positions; close to the head, close to the coil, and between the head and the RF coil to investigate the areas where the B_1^+ can be affected. The DL positions relative to the coil are shown in Fig. 1(a). Furthermore, in our simulation setups, the effect of DLs was investigated at two different angles or configurations (“A” and “B”). For DLs’ lossy and lossless condition, various σ values (0.0001 S/m and 0.5 S/m, and 1 S/m) were used. Moreover, the head SAR was calculated for $\varepsilon_r = 78$ value of the DL and plotted in axial, coronal, and sagittal slices. To assess the SNR of RF coil arrays, MUSAIK V2.0 was used for simulations. The MUSAIK provides SNR and parallel imaging capabilities by importing the simulation results. For the Duke head model, the total number of mesh cells (voxel size) over the entire simulation volume amounted to 11.249 million cells, and 0.5 spatial resolution was used for simulations.

The axial, sagittal, and coronal slices were used as the target slices to depict the field distributions inside the head for the B_1^+ improvement and performance comparison at 7 T, as shown in Fig. 1(a). The anatomically *Duke* head model was used as a load in Sim4Life for the RF coil simulations. In this paper, three optimization parameters were evaluated in the head slice. The first parameter is the B_1^+ $T_{x,eff}$, which can be measured in $\mu T/\sqrt{W}$ and defined by:

$$T_{Xeff} = \mu/\sqrt{P_{in}} \tag{1}$$

where μ is the mean value of the B_1^+ and P_{in} is the total input power. All the B_1^+ fields were calculated based on the simulated input power of 8 W. We kept a 45° phase shift between the adjacent channel of the MTL transmit array. The second parameter is the CV = (standard deviation (B_1^+) / μ), while the third parameter is the peak 10g-averaged SAR value in W/kg. The spatially averaged SAR values were evaluated in Sim4Life using the psSAR[IEEE/IEC62704-1] averaging method.

B. RF-SHIMMING OR MATLAB OPTIMIZATION ROUTINE

A routine was implemented in Matlab to achieve the higher B_1^+ homogeneity and minimize the 10-g peak SAR values

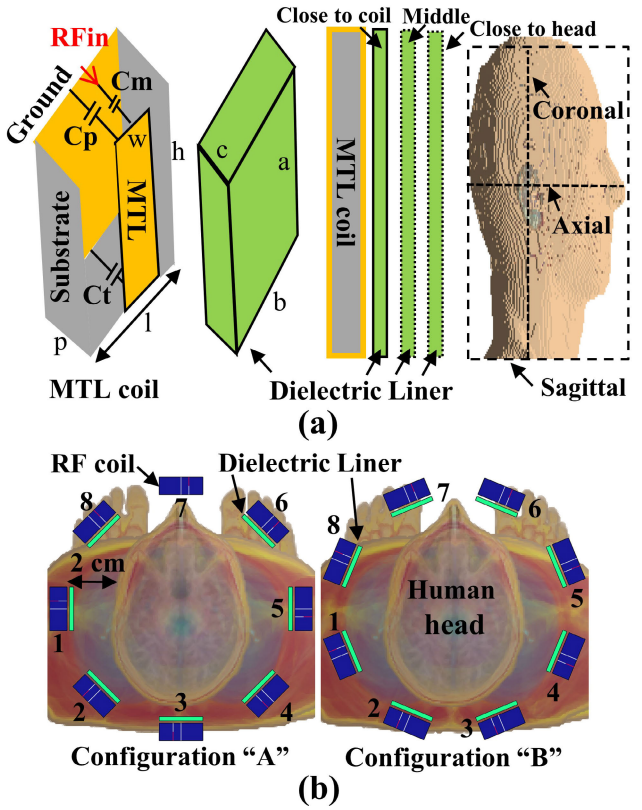

FIGURE 1. (a) Design of the single-element MTL transmit RF coil and DL. (b) Simulation setups for the configurations "A" and "B" showing the RF coil and high dielectric liner (DLs) positions around the head. The DL position could be one of the three positions. The diameter of the cylinder on which the MTL elements are mounted is 26 cm. Summary of the dimensions are as follows: $a = 15$, $b = 5$, $c = 0.5$, $h = 15$, $l = 5$, $p = 2$, $w = 1.8$ (Units: centimeters).

within the head slices (axial, sagittal, and coronal). The RF-shimming optimization [6] was used with the MTL transmit array RF coil and DLs. Herein, the RF-shimming optimization was applied by designing the phase and amplitude of the excitation. The optimal solution for the phase and amplitude can be solved using a multi-iterations routine implemented in Matlab [32]. The optimization routine started with the initial 16 optimization variables with uniform amplitudes and a 45° phase shift. After finding the optimum value for the input power (in W) and the phase of the input source, the RF shimming results were incorporated in the post-processing step.

C. BENCH MEASUREMENT SETUPS AND MRI

Finally, the MTL transmit array coil was fabricated to measure the S-parameters and magnetic field. Fig. 2(a) illustrates the developed eight-element RF coil prototype without and with the DL. In the setup, the MTL transmit array was mounted on a Teflon substrate, and two V9000 variable capacitors (C_m and C_t) were used. These V9000 capacitors are specifically used in the implementation of MRI RF coils. The Voltronics manufacturer provides the non-trimmer capacitors in the range of 1 pF to 10 pF. On the posterior side of the Teflon, the ground was attached to provide the

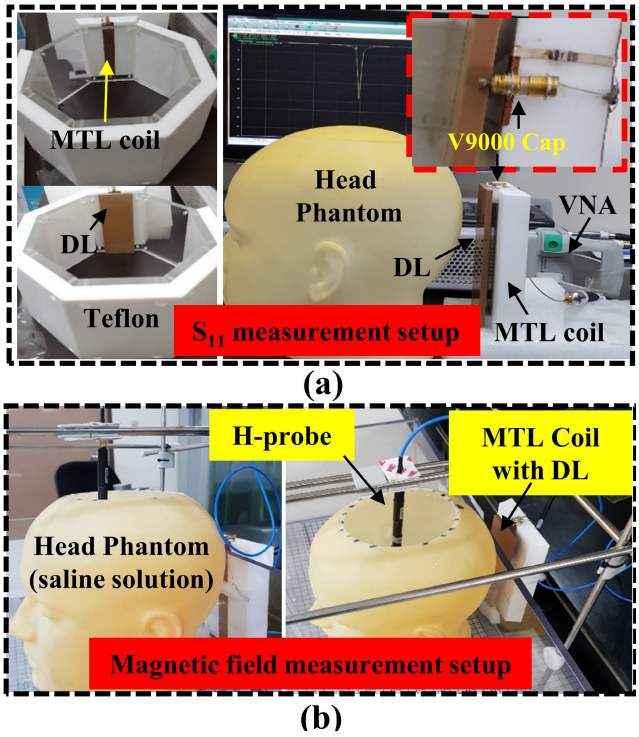

FIGURE 2. Measurement setups of the transmit array coil. (a) S_{11} measurement. (b) Magnetic field measurement using H-probe. A commercial DL made of BaSmTi oxide composition (E5080, EXXELIA^{TEMEX}) and an H-probe connected to a signal generator (MS2830A, Anritsu) were used for measurement. Deionized water, sugar, and salt (NaCl) were used in the preparation of saline solution to imitate the human brain properties.

current loop in the coil. For the validation of the simulated results, a commercial DL made of BaSmTi oxide composition (E5080, EXXELIA^{TEMEX}) was fabricated, as shown in Fig. 2(a). The matching and tuning of the RF coil at 7 T without and with the DL was found by changing the knob of the V9000 variable capacitors. For the magnetic field measurement, a single channel of the array coil and an H-probe connected to a signal generator (MS2830A, Anritsu) was used, as shown in Fig. 2(b). The H-probe was located inside the head phantom filled with a saline solution, and the magnetic field was measured at various points. Deionized water, sugar, and salt (NaCl) were used in the preparation of saline solution to imitate the human brain properties. The magnitude of the magnetic field was calculated by collecting the H_x, and H_y components of the field at every point using the H-probe. The field was measured in 10 cm × 10 cm and normalized to the maximum value.

A specific slice selective gradient recalled echo (GRE) sequence was used with a 2.5 ms (T1-weighted) and 100 ms (T2-weighted) echo time (TE), a 500 ms (T1-weighted), and 3000 ms (T2-weighted) relaxation/repetition time (TR), a 30° flip angle, a 128 × 128 image acquisition matrix, a 2 mm slice thickness, and a 23 cm × 23 cm field-of-view (FOV) to obtain the MR images. These parameters were fed into a Bloch simulator described in [33] to generate all the MR images with the MTL numerically. An axial slice was used to

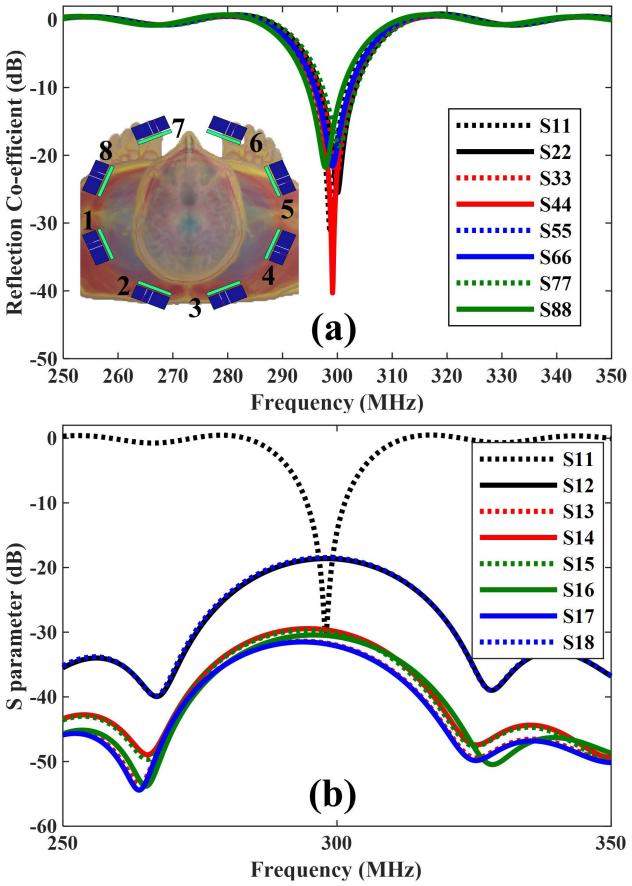

FIGURE 3. Simulated S-parameters of the eight-channel transmit array coil. (a) Reflection coefficients. (b) Transmission coefficients. The reflection coefficients of all elements are lower than −20 dB, while the transmission coefficients between the MTL array coil's adjacent elements were achieved lower than −15 dB.

target the center of the head model for the MR images of the eight-element MTL coil.

III. RESULTS AND DISCUSSION

A. EM SIMULATIONS FOR EIGHT-ELEMENT RF COIL WITH DL

To investigate the effects of DLs in the heterogeneous head phantom and achieve realistic results, the eight-element RF coil and DLs were simulated using the FDTD-based Sim4Life. All the MTL transmits array coil elements are tuned and matched at the 7 T resonance frequency (298 MHz), as shown in Fig. 3(a). The return loss value of all elements is lower than −20 dB. The coupling between the MTL transmit array coil's adjacent elements was achieved lower than −15 dB, as shown in Fig. 3(b). After loading the DL in the RF coil environment, the high ε_r value of the DL detuned the coil's resonant frequency. Hence, the variable capacitor C_t value was changed to retune the RF coil at 298 MHz.

We computed the field distributions without the DLs ($B_1^{+;no\,DL}$) and with the DLs (B_1^+) at the target slices. The primary purpose of using DL with the MTL coil was to

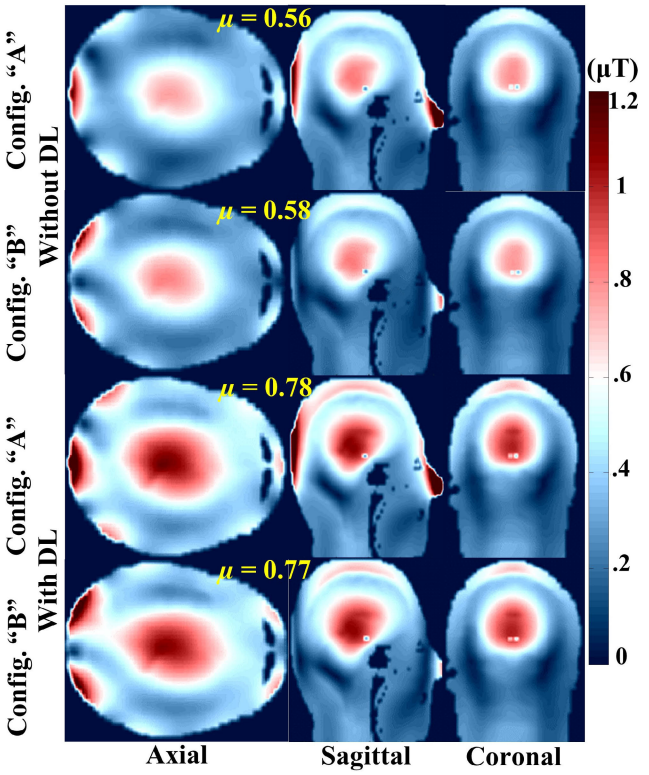

FIGURE 4. The simulated axial B_1^+ field distributions within the *Duke* head model for the eight-element MTL transmit array coil without and with the DL at both coil configurations. The DL size of 5 cm × 15 cm × 0.5 cm was used for $T_{x,eff}$ and relative standard deviation (CV) calculation. μ is the mean of the B_1^+ in the head slice. All the B_1^+ fields were calculated based on the simulated input power of 8 W.

maximize the transmit field intensity in a particular region (center of the head). Fig. 4 illustrates the simulated axial, sagittal, and coronal slices of the B_1^+ field within the *Duke* head model for the MTL transmit array coil without and with the DL. The DLs improved the $T_{x,eff}$ in the head slices and minimized the field inhomogeneity. After using the DLs with MTL transmit array coil, the higher central B_1^+ values were pronounced at the center of the head with maximum B_1^+ intensity. The results showed that the DL with MTL coil improved the $T_{x,eff}$ by 39% in the head compared to the case without DL. It can be observed from the figure that the μ value in the head slices for configurations "A" was increased from 0.56 μT to 0.78 μT. For configuration "B", the μ value in the head was improved from 0.58 μT to 0.77 μT. Additionally, the CV value was decreased from 0.37 to 0.32 using DLs, which showed that the DLs case provided homogeneous field distribution. Using the DLs not merely increases the B_1^+ field in the center of the head but increases the field strength in the whole head slice as well, resulting in the improvement of field homogeneity throughout the slice. All the numerical values of the μ, $T_{x,eff}$, and CV are summarized in Table 2. The DLs provide additional B_1^+ strength due to the displacement current (J_d), leads to power balancing, reduced tissue dissipated power, and destructive cancellation of field components inside the head. The DLs act as absorbing layers,

TABLE 2. Summary of the simulated μ field in μT, Tx_{eff} in $\mu T/\sqrt{W}$, and CV in the head slice with DL. The MTL array coil was fed with the simulated power of 8 W.

Simulation setup			μ	Tx_{eff}	CV
Configuration "B" 5mm DL		w/o DL	0.58	0.205	0.36
		with DL (Close to coil)	0.77	0.272	0.32
Configuration "A" 5mm DL		w/o DL	0.56	0.198	0.37
		With DL (Close to coil)	0.78	0.276	0.32
Configuration "A"	5 mm	Close to head	0.61	0.216	0.36
	5 mm	Middle of head and coil	0.64	0.227	0.35
	5 mm	Close to RF coil	0.78	0.276	0.32
	10 mm	DL thickness	0.69	0.244	0.34
	5 mm	Lossy ($\sigma = 0.5$)	0.66	0.233	0.35
	5 mm	RF Shimming w/o DL	0.53	0.187	0.31
	5 mm	RF Shimming with DL	0.75	0.265	0.29

which eliminate the reflected waves from the object's surface and boundaries between tissues. Therefore, they reduce the effect of destructive interference, which shapes a conservative E-field and thereby improves the B_1^+ field in the head.

Furthermore, the comparison of the B_1^+ distributions for the DLs with thicknesses of 0.5 cm and 1 cm was carried out for configuration "A". Fig. 5(a) illustrates the axial B_1^+ distributions within the *Duke* head model. The DLs with a thickness of 0.5 cm provided better field improvement than those with a thickness of 1 cm. For the DL with a thickness of 1 cm, the $T_{x,eff}$ value in the head slice was improved approximately 23%, while the improvement value for 0.5 cm thickness was 39%. Moreover, the B_1^+ distributions were compared for the DLs with thicknesses of 0.5 cm positioned close to the head model, in the middle of the RF coil elements and the head model, and close to the RF coil, as shown in Fig. 5(c). At the corresponding DLs positions, the $T_{x,eff}$ values in the head slice were improved by about 9%, 15%, and 39%, respectively. From these values, it is worth noting that the thinner DLs near the RF coil performed better in the field improvement. Table 2 summarizes the numerical field-values comparison at DL thicknesses for the different positions relative to the RF coil and head.

Fig. 5(b) displays the axial B_1^+ distributions within the *Duke* head model for $\sigma = 0.5$ S/m. From the B_1^+ distributions, the $T_{x,eff}$ value in the head slice was improved by approximately 18%. This value showed that the lossless condition ($\sigma = 0.0001$ S/m) provided improved $T_{x,eff}$ (39%) within the head model, whereas, at the lossy condition ($\sigma = 0.5$ S/m, 1 S/m) the field improvement was less effective. At $\sigma =$ 1 S/m, the field improvement becomes negligible. A parametric study was carried out to further justify the DL of 0.5 cm thickness by simulating DLs with different thicknesses from 10 mm to 1 mm. From all simulations and B_1^+ distributions, DLs with the optimal thickness of 0.5 cm showed better RF coil performance and yield the maximum field distribution in the head.

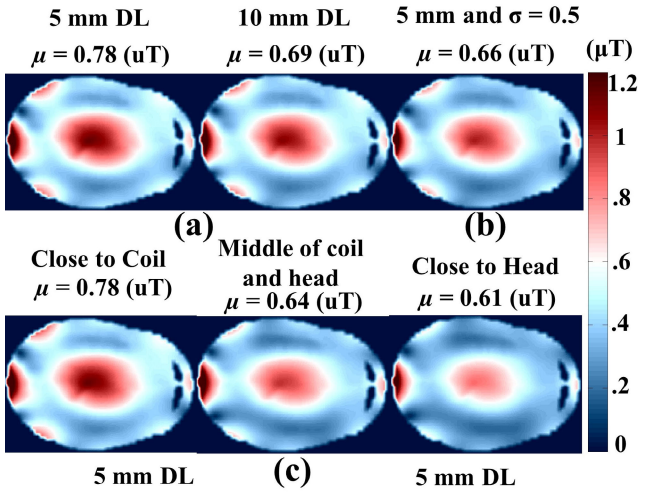

FIGURE 5. Comparison of the simulated axial B_1^+ field distributions within the *Duke* head model. (a) 0.5 cm and 1 cm DLs thickness. (b) 0.5 cm lossy DL. (c) At three different DL positions. (d) Field strength variation with DL thickness variation spanning a spatial range from 10 mm to 1 mm.

B. RF SHIMMING WITHOUT AND WITH THE DLs

For the homogeneous field distributions in the head, the optimum values of the applied source and phase were selected for each element in the multi-element RF configuration "A". Fig. 6 (upper row) displays the RF shimmed B_1^+ distributions within the head of the *Duke* model at axial, sagittal, and coronal slice. The CV value decreased from 0.37 to 0.32 in the target head slices. The value shows that the technique improved the B_1^+ homogeneity.

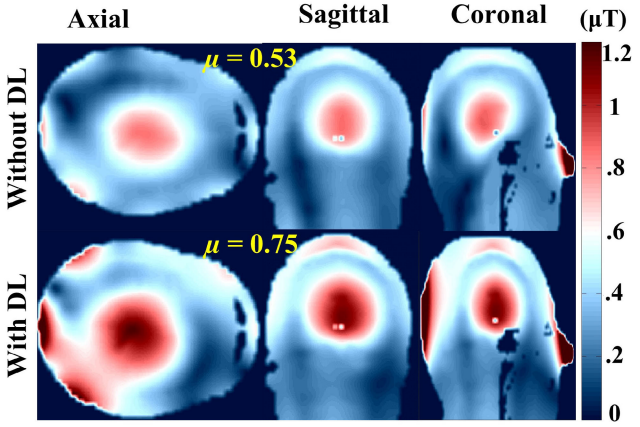

FIGURE 6. Simulated RF shimmed B_1^+ field distributions within the *Duke* head model for the MTL transmit array coil. The DL size of 5 cm and configuration "A" were used for $T_{x,eff}$ and relative standard deviation (CV) calculation. μ is the mean of the B_1^+ in the head slice.

After achieving the RF shimmed B_1^+, the DLs were introduced to improves the $T_{x,eff}$ in the head of the *Duke* model and to minimize the RF field interference. Fig. 6 (lower row) displays the simulated $T_{x,eff}$ of the RF shimmed B_1^+ produced

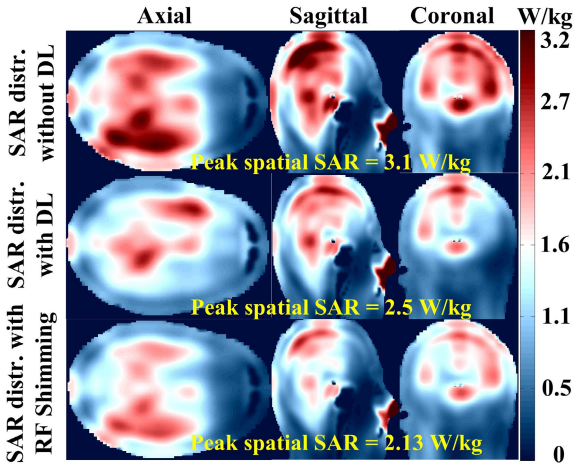

FIGURE 7. Simulated peak 10g-averaged SAR comparison in the selected slices for the MTL coil without and with the DLs and using the RF shimming. Using the DLs and RF-shimming, the SAR value is reduced from 3.1 W/kg to 2.13 with reduced SAR distribution at the temporal lobe of the brain.

by the eight-element RF coil with DLs within the *Duke* head model. The higher signal intensity in the head slices was achieved using the DLs than the case without DLs. It can be observed from the simulation results that the insertion of DLs in the RF coil setup achieved an improvement of 42% in the $T_{x,eff}$ in the target slices of the head model. The field distributions at the target slices were more intense in the head, and the μ value was improved from 0.53 μT to 0.75 μT. The RF-shimming technique and the DLs improved the B_1^+ homogeneity by approximately 21%, and the CV value was decreased from 0.37 to 0.29 in the target head slices. All the numerical values of the μ, $T_{x,eff}$, and CV for the RF shimming technique without and with the DLs are summarized in Table 2. The values show that the DL is effective in the head model, and the field distribution is improved in the target slices.

C. SAR OF MTL COIL WITH DLs

To ensure the safety of MRI patients, the IEC/FDA has restricted the peak 10g-averaged SAR for the head tissues to 3.2 W/kg. The presented SAR values in the head tissues are the peak 10-g SAR, calculated for the MTL coil with the input power of 1 W for each channel (total 8 W). The compared SAR distributions for MTL coil without and with the DLs are plotted in Fig. 7. The MTL transmit array coil without a DL produced 3.1 W/kg SAR in the head, which complies with the standard limiting value of the head SAR in MRI. The higher SAR distributions were observed at the temporal lobe of the brain due to its closer distance to the transmits array coil. Therefore, the DLs were inserted to reduce the higher SAR distribution. From the sensor's SAR distribution, it was observed that the MTL coil with DLs produced a peak SAR value of 2.5 W/kg. The above value shows that the peak SAR is reduced in the head slice when a DL is used. In our proposed configuration, the RF-shimming technique was also used to minimize the SAR in the head. After using the

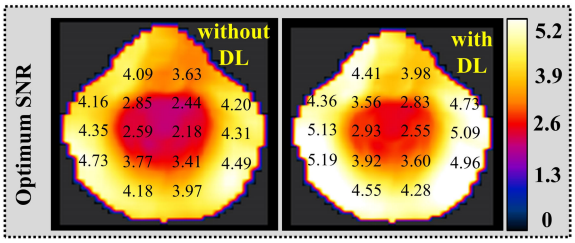

FIGURE 8. Optimum SNR of the eight-element RF coil without and with the DLs. The SNR strength is plotted at every pixel region of the slice.

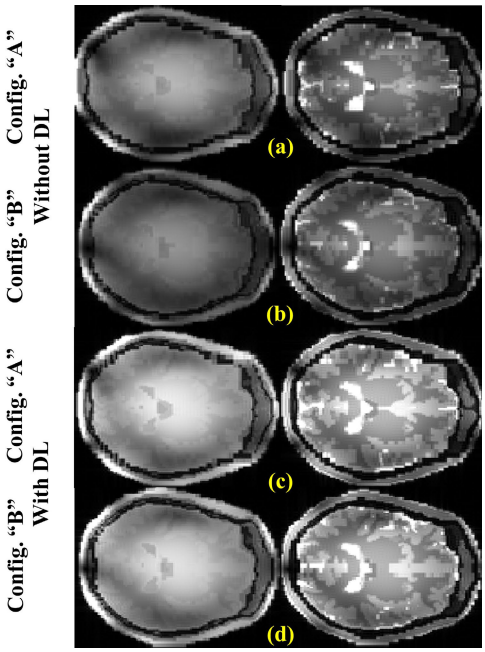

FIGURE 9. T1-weighted and T2-weighted MR images acquired from the eight-element RF coil and DLs at 7 T. Constant TE of 3 ms for T1-weighted and 100 ms for T2-weighted, TR of 500 ms for T1-weighted, and 3000 ms for T2-weighted, and a flip angle of 30°, were used with the GRE sequence. The first image is T1-weighted, whereas the second image is T2-weighted. (a)–(b) Without DLs. (c)–(d) With DLs.

RF-shimming, the peak SAR value was reduced to 2.13 W/kg in the head, and lower SAR distributions were achieved at the temporal lobe areas of the slices. The figure shows the case where the DLs and the RF shimming was used to yield the minimum SAR values in the head. It is observed that the RF-shimming and DLs provided the best B_1^+ homogeneity and improved $T_{x,eff}$ field values with minimal peak SAR values in the head.

D. OPTIMUM SNR

The optimum SNR strength at every pixel without and with the DLs is illustrated in Fig. 8. It can be seen that the optimum SNR at the temporal or side area of the brain is a bit lower and darker without DL, whereas much higher and brighter SNR is achieved after the insertion of DL in the coil setup. The field slice shows that the optimum SNR is improved and increased in every region of the head slice. The numerical values at different regions over the transverse slice are also plotted. The

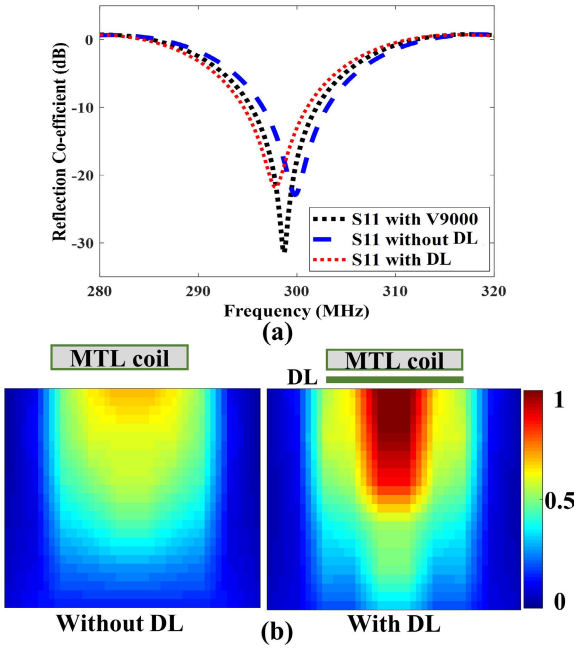

FIGURE 10. Measurement results of the transmit array without and with the DL. (a) Measured S_{11}. (b) Measured field maps. The measured S-parameter results were obtained using the fabricated MTL array coil and DL, whereas the field maps were measured using the H-probe.

slice SNR intensity obtained from both colors and numerical values shows that the DLs provide better optimum SNR over the entire area of the transverse slice. In this figure, the optimum SNR is improved by inserting DLs. Correspondingly, the comparison depicts the effectiveness of the DLs.

E. SIMULATED MRI ACQUISITIONS

A single simulated GRE sequence was used to obtain the MR images of the MTL transmit array coil without and with the DL. Fig. 9 shows the MR image comparison without and with the DLs at the center axial slice. The method described in [33] was used to numerically generate all the MR images with the MTL coil at 7 T. The results show that the images provide higher signal intensity, and the DLs pronounced bright field distributions at the head model compared to the images without DLs. The tissues were visualized in the MR image using the DLs, and the intensity of the image at the center was more intense than the images without DLs. Moreover, the images acquired in the head model reflect the stronger B_1^+ homogeneity in the center of the head and show relatively better SNR compared to the images without DLs. The measured T1-weighted and T2-weighted MR images show that B_1^+ is considerably improved locally by the introduction of the DLs, which corresponds to an enhanced contrast homogeneity throughout the axial slices.

F. BENCH MEASUREMENT RESULTS

Fig. 10(a) shows the measured reflection coefficients of the transmit array coil without and with the DL. It can be observed that the measurement setup provides the desired reflection coefficient results. The coil is matched to about −30 dB and tuned at 298 MHz. The figure shows that the coil resonates at our desired frequency with a little variation in the S_{11} owing to the DL loading in the setup. Fig. 10(b) depicted the measured field maps of the RF array coil without and with the DL. The measured field maps show that the case with the DL provides higher field intensity than without the DL case. When the DL was inserted, the field propagates deeper in the head with higher intensity. The measured results are in good agreement with the simulation results; thus, the proposed DL is a promising solution for field improvement.

IV. CONCLUSION

In this study, an eight-element MTL transmits array head coil was used with small DLs at 7 T. The proposed RF coil and DLs were placed around the head in two configurations (“A” and “B”). Multiple dimensions of the DL thickness were simulated for selecting the optimum thickness. From all simulation results, it was observed that the DLs provided 39% $T_{x,eff}$ improvement in the selected head slices compared to the case without DLs. The RF-shimming technique and DLs improved the B_1^+ homogeneity for the MTL transmit array coil with DLs by 21% in the central axial slice. The peak SAR in the head slices was minimized by DLs and RF-shimming. The proposed DLs improved the MRI images and modified the distribution of the RF electromagnetic fields. Hence, the DL materials with multi-element MTL transmit coils can enhance the transmitted field in the head model and improve the field distribution in the deep target region. Therefore, these materials can be the best candidate to use in the MRI system to obtain higher resolution images of the patients.

REFERENCES

[1] C. E. Akgun, L. Delabarre, H. Yoo, S. M. Sohn, C. J. Snyder, G. Adriany, K. Ugurbil, A. Gopinath, and J. T. Vaughan, “Stepped impedance resonators for high-field magnetic resonance imaging,” *IEEE Trans. Biomed. Eng.*, vol. 61, no. 2, pp. 327–333, Feb. 2014.
[2] H. David and D. Phil, “Sensitivity and power deposition in a high-field imaging experiment,” *J. Magn. Reson. Imag.*, vol. 12, no. 1, pp. 46–67, 2000.
[3] J. T. Vaughan, M. Garwood, C. M. Collins, W. Liu, L. DelaBarre, G. Adriany, P. Andersen, H. Merkle, R. Goebel, M. B. Smith, and K. Ugurbil, “7T vs. 4T: RF power, homogeneity, and signal-to-noise comparison in head images,” *Magn. Reson. Med., Off. J. Int. Soc. Magn. Reson. Med.*, vol. 46, no. 1, pp. 24–30, 2001.
[4] A. M. Abduljalil, A. Kangarlu, X. Zhang, R. E. Burgess, and P.-M.-L. Robitaille, “Acquisition of human multislice MR images at 8 Tesla,” *J. Comput. Assist. Tomogr.*, vol. 23, no. 3, pp. 335–340, May 1999.
[5] X. Zhang, K. Ugurbil, and W. Chen, “Microstrip RF surface coil design for extremely high-field MRI and spectroscopy,” *Magn. Reson. Med.*, vol. 46, no. 3, pp. 443–450, 2001.
[6] H. Yoo, A. Gopinath, and J. T. Vaughan, “A method to localize RF B_1 field in high-field magnetic resonance imaging systems,” *IEEE Trans. Biomed. Eng.*, vol. 59, no. 12, pp. 3365–3371, Dec. 2012.
[7] I. A. Elabyad, T. Herrmann, C. Bruns, J. Bernarding, and D. Erni, “RF shimming and improved SAR safety for MRI at 7 T with combined eight-element stepped impedance resonators and traveling-wave antenna,” *IEEE Trans. Microw. Theory Techn.*, vol. 66, no. 1, pp. 540–555, Jan. 2018.
[8] G. Adriany, P.-F. Van de Moortele, J. Ritter, S. Moeller, E. J. Auerbach, C. Akgün, C. J. Snyder, T. Vaughan, and K. Uğurbil, “A geometrically adjustable 16-channel transmit/receive transmission line array for improved RF efficiency and parallel imaging performance at 7 Tesla,” *Magn. Reson. Med.*, vol. 59, no. 3, pp. 590–597, Mar. 2008.

[9] G. Adriany, E. J. Auerbach, C. J. Snyder, A. Gözübüyük, S. Moeller, J. Ritter, P.-F. Van de Moortele, T. Vaughan, and K. Uğurbil, "A 32-channel lattice transmission line array for parallel transmit and receive MRI at 7 Tesla," *Magn. Reson. Med., Off. J. Int. Soc. Magn. Reson. Med.*, vol. 63, no. 6, pp. 1478–1485, 2010.

[10] X. Yan, J. O. Pedersen, L. Wei, X. Zhang, and R. Xue, "Multichannel double-row transmission line array for human MR imaging at ultra-high fields," *IEEE Trans. Biomed. Eng.*, vol. 62, no. 6, pp. 1652–1659, Jun. 2015.

[11] S.-M. Sohn, L. DelaBarre, A. Gopinath, and J. T. Vaughan, "RF head coil design with improved RF magnetic near-fields uniformity for magnetic resonance imaging (MRI) systems," *IEEE Trans. Microw. Theory Techn.*, vol. 62, no. 8, pp. 1784–1789, Aug. 2014.

[12] Y. Cho, A. Basir, and H. Yoo, "Adjustable RF transmitter head coil: Improving transmit efficiency with SAR management for 7-T magnetic resonance imaging," *IEEE Trans. Microw. Theory Techn.*, vol. 69, no. 5, pp. 2686–2696, May 2021.

[13] Y. Takayama, H. Nonaka, M. Nakajima, T. Obata, and H. Ikehira, "Reduction of a high-field dielectric artifact with homemade gel," *Magn. Reson. Med. Sci.*, vol. 7, no. 1, pp. 37–41, May 2008.

[14] Q. X. Yang, W. Mao, J. Wang, M. B. Smith, H. Lei, X. Zhang, K. Ugurbil, and W. Chen, "Manipulation of image intensity distribution at 7.0 T: Passive RF shimming and focusing with dielectric materials," *J. Magn. Reson. Imag.*, vol. 24, no. 1, pp. 197–202, 2006.

[15] W. M. Teeuwisse, W. M. Brink, K. N. Haines, and A. G. Webb, "Simulations of high permittivity materials for 7 T neuroimaging and evaluation of a new barium titanate-based dielectric," *Magn. Reson. Med.*, vol. 67, no. 4, pp. 912–918, 2012.

[16] M. Kataoka, H. Isoda, Y. Maetani, Y. Nakamoto, T. Koyama, S. Umeoka, K. Tamai, A. Kido, N. Morisawa, T. Saga, and K. Togashi, "MR imaging of the female pelvis at 3 Tesla: Evaluation of image homogeneity using different dielectric pads," *J. Magn. Reson. Imag.*, vol. 26, no. 6, pp. 1572–1577, 2007.

[17] W. M. Brink, A. M. van der Jagt, M. J. Versluis, B. M. Verbist, and A. G. Webb, "High permittivity dielectric pads improve high spatial resolution magnetic resonance imaging of the inner ear at 7 T," *Invest. Radiol.*, vol. 49, no. 5, pp. 271–277, 2014.

[18] V. Vorobyev, A. Shchelokova, I. Zivkovic, A. Slobozhanyuk, J. D. Baena, J. P. del Risco, R. Abdeddaim, A. Webb, and S. Glybovski, "An artificial dielectric slab for ultra high-field MRI: Proof of concept," *J. Magn. Reson.*, vol. 320, Nov. 2020, Art. no. 106835.

[19] P. de Heer, W. M. Brink, B. J. Kooij, and A. G. Webb, "Increasing signal homogeneity and image quality in abdominal imaging at 3 T with very high permittivity materials," *Magn. Reson. Med.*, vol. 68, no. 4, pp. 1317–1324, Oct. 2012.

[20] P. de Heer, M. B. Bizino, M. J. Versluis, A. G. Webb, and H. J. Lamb, "Improved cardiac proton magnetic resonance spectroscopy at 3 T using high permittivity pads," *Investigative Radiol.*, vol. 51, no. 2, pp. 134–138, Feb. 2016.

[21] K. Haines, N. B. Smith, and A. G. Webb, "New high dielectric constant materials for tailoring the $B1^+$ distribution at high magnetic fields," *J. Magn. Reson.*, vol. 203, no. 2, pp. 323–327, Apr. 2010.

[22] Q. X. Yang, J. Wang, J. Wang, C. M. Collins, C. Wang, and M. B. Smith, "Reducing SAR and enhancing cerebral signal-to-noise ratio with high permittivity padding at 3 T," *Magn. Reson. Med.*, vol. 65, no. 2, pp. 358–362, Feb. 2011.

[23] J. E. M. Snaar, W. M. Teeuwisse, M. J. Versluis, M. A. van Buchem, H. E. Kan, N. B. Smith, and A. G. Webb, "Improvements in high-field localized MRS of the medial temporal lobe in humans using new deformable high-dielectric materials," *NMR Biomed.*, vol. 24, no. 7, pp. 873–879, Aug. 2011.

[24] J. H. F. Van Gemert, W. Brink, A. Webb, and R. Remis, "An efficient methodology for the analysis of dielectric shimming materials in magnetic resonance imaging," *IEEE Trans. Med. Imag.*, vol. 36, no. 2, pp. 666–673, Feb. 2016.

[25] A. Kordzadeh and N. De Zanche, "Optimal-permittivity dielectric liners for a 4.7 T transceiver array," *Magn. Reson. Imag.*, vol. 48, pp. 89–95, May 2018.

[26] M. M. Garcia, K. T. Chaim, M. C. G. Otaduy, A. Rennings, D. Erni, M. Vatanchi, and W. Zylka, "Investigating the influence of dielectric pads in 7T magnetic resonance imaging–simulated and experimental assessment," *Current Directions Biomed. Eng.*, vol. 6, no. 3, pp. 24–27, Sep. 2020.

[27] A. Kordzadeh and N. D. Zanche, "Control of mutual coupling in high-field MRI transmit arrays in the presence of high-permittivity liners," *IEEE Trans. Microw. Theory Techn.*, vol. 65, no. 9, pp. 3485–3491, Sep. 2017.

[28] A. Maunder, N. D. Zanche, and A. K. Iyer, "Simulation comparison of birdcage coil and metamaterial liner for MRI at 3T and 4.7T," in *Proc. 50th Eur. Microw. Conf. (EuMC)*, Jan. 2021, pp. 1067–1070.

[29] M. V. Vaidya, M. Lazar, C. M. Deniz, G. G. Haemer, G. Chen, M. Bruno, D. K. Sodickson, R. Lattanzi, and C. M. Collins, "Improved detection of fMRI activation in the cerebellum at 7T with dielectric pads extending the imaging region of a commercial head coil," *J. Magn. Reson. Imag.*, vol. 48, no. 2, pp. 431–440, Aug. 2018.

[30] V. Vorobyev, A. Shchelokova, A. Efimtcev, J. D. Baena, R. Abdeddaim, P. Belov, I. Melchakova, and S. Glybovski, "Improving B1 homogeneity in abdominal imaging at 3 T with light and compact metasurface," 2021, *arXiv:2102.01384*. [Online]. Available: https://arxiv.org/abs/2102.01384

[31] A. Christ, W. Kainz, E. G. Hahn, K. Honegger, M. Zefferer, E. Neufeld, W. Rascher, R. Janka, W. Bautz, J. Chen, B. Kiefer, P. Schmitt, H.-P. Hollenbach, J. Shen, M. Oberle, D. Szczerba, A. Kam, J. W. Guag, and N. Kuster, "The virtual family—Development of surface-based anatomical models of two adults and two children for dosimetric simulations," *Phys. Med. Biol.*, vol. 55, no. 2, pp. N23–N38, Jan. 2010.

[32] C. Olson, H. Yoo, L. Delabarre, J. T. Vaughan, and A. Gopinath, "RF B_1 field localization through convex optimization," *Microw. Opt. Technol. Lett.*, vol. 54, no. 1, pp. 31–37, Jan. 2012.

[33] Z. Cao, S. Oh, C. T. Sica, J. M. McGarrity, T. Horan, W. Luo, and C. M. Collins, "Bloch-based MRI system simulator considering realistic electromagnetic fields for calculation of signal, noise, and specific absorption rate," *Magn. Reson. Med.*, vol. 72, no. 1, pp. 237–247, Jul. 2014.

SANA ULLAH received the B.Sc. and M.Sc. degrees in telecommunication engineering from the University of Engineering and Technology, Peshawar, Pakistan, in 2013 and 2016, respectively. He is currently pursuing the Ph.D. degree in electronic engineering with Hanyang University, Seoul, South Korea. His current research interests include 60 GHz MIMO antennas, implantable antennas, metamaterial, RF coils for MRI, microcoil for blood vessel imaging, flexible and stretchable RF coils, and sensors with MRI receive coil. In 2018, he was awarded for the best student paper by the Korean Institute of Electromagnetic Engineering and Science (KIEES). He has been the Samsung Foundation Global Hope Scholar, since 2018.

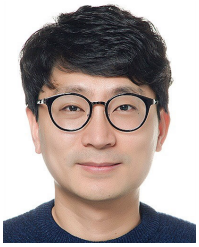

HYOUNGSUK YOO (Senior Member, IEEE) received the B.Sc. degree in electrical engineering from Kyungpook National University, Daegu, South Korea, in 2003, and the M.Sc. and Ph.D. degrees in electrical engineering from the University of Minnesota, Minneapolis, MN, USA, in 2006 and 2009, respectively.

In 2009, he joined the Center for Magnetic Resonance Research, University of Minnesota, as a Postdoctoral Associate. In 2010, he joined Cardiac Rhythm Disease Management, Medtronic, MN, USA, as a Senior Electromagnetic (EM)/MRI Scientist. From 2011 to 2018, he was an Associate Professor with the Department of Biomedical Engineering, School of Electrical Engineering, University of Ulsan, Ulsan, South Korea. Since 2018, he has been an Associate Professor with the Department of Biomedical Engineering and the Department of Electronic Engineering, Hanyang University, Seoul, South Korea. He has been the CEO of Electromagnetics and Magnetic Resonance (E2MR), a startup company, since 2017. His current research interests include EM theory, numerical methods in EMs, metamaterials, antennas, implantable devices, and magnetic resonance imaging in high-magnetic field systems. He was awarded the Third Prize for the Best Student Paper at the 2010 IEEE Microwave Theory and Techniques Society International Microwave Symposium.